



CHORUS

This is the accepted manuscript made available via CHORUS. The article has been published as:

## Thermophoretically modified aerosol Brownian coagulation

Manuel Arias-Zugasti and Daniel E. Rosner

Phys. Rev. E **84**, 021401 — Published 5 August 2011

DOI: [10.1103/PhysRevE.84.021401](https://doi.org/10.1103/PhysRevE.84.021401)

# Thermophoretically-Modified Aerosol Brownian Coagulation

Manuel Arias-Zugasti<sup>1,2\*</sup> and Daniel E. Rosner<sup>2†</sup>

<sup>1</sup>*Dept. de Física Matemática y de Fluidos, UNED, Apdo : 60141, 28080 Madrid, Spain and*

<sup>2</sup>*Chemical & Environmental Engineering Dept., Yale University, New Haven, CT 06520-8286, USA*

A theory of aerosol coagulation rates resulting from continuum-regime Brownian coagulation in the presence of size-dependent particle thermophoresis is developed and explored here. We are motivated by a wide variety of applications in which particle Brownian coagulation occurs in a non-isothermal gas where differential thermophoretic drift contributes to, but does not dominate, the encounter frequency between suspended spherical particles (e.g. mist droplets) of different size. We employ a Smoluchowski-like population-balance to demonstrate the relative roles of Brownian diffusion and thermophoresis in shaping the short- and long- time (asymptotic or “coagulation-aged”-) mist-droplet size distribution (DSD) function. To carry out these combined mechanism DSD-evolution calculations we developed a rational “coupled” coagulation rate constant (allowing for simultaneous Brownian diffusion and relative thermophoretic drift) rather than simply adding the relevant individual coagulation “kernels”. Dimensionless criteria are provided to facilitate precluding other coagulation mechanisms not considered here (such as : simultaneous sedimentation or Marangoni-flow induced mist droplet phoresis) and potential complications not included in the present model (as finite-rate coalescence, initial departures from the continuum (Stokes drag-) limit, and even dense (non-ideal) vapor effects).

---

\* maz@dfmf.uned.es

† daniel.rosner@yale.edu

## I. INTRODUCTION, MOTIVATION, BACKGROUND, OBJECTIVES

Except in the free-molecule limit, aerosols (comprised of spherical solid(-like) particles or “mist” droplets) finding themselves in a non-isothermal carrier gas will drift at different speeds because of size differences. This may be regarded as the result of “biased” Brownian motion, and such situations are now known to occur in many materials processing and energy technologies (see, e.g., Rosner (2011) [1]). In some cases (especially metallurgical process engineering, cutting and welding operations, and in certain accident scenarios, e.g., spilled molten metal- or salt- coolants) we recently found that thermophoretic drift can actually dominate [2, 3] ordinary isotropic Brownian coagulation—providing a natural limiting-case to initiate the exploration of this previously overlooked coagulation mechanism (Rosner and Arias-Zugasti (2011) [4]). In the present extension, we now turn our attention to those more common environments in which particle Brownian coagulation occurs in a non-isothermal gas and differential thermophoretic drift contributes to, but does not initially dominate, the encounter frequency between suspended spherical particles of different size in a dilute (low volume fraction-) suspension. When the carrier gas mean-free-path ( $\ell$ ) is small compared to the initial Sauter mean diameter (SMD) for the coagulating population, this may be realized because of “modest” : local temperature gradients (e.g.  $< 10^5$  K/m), and/or : prevailing particle/gas thermal conductivity ratios (e.g. not much above 10-fold). If particle coagulation persists in such an environment we ask : How will the presence of this thermophoretic drift mechanism accelerate the associated reduction in particle number density, and distort the evolving size distribution function ?

With these questions in mind, the present paper has been structured as follows : In Section II we summarize the essential features of our present mathematical model—i.e. the physical assumptions to be exploited in Sections III-V and discussed and defended in Section VI. Section III is devoted to the rational development of a coagulation rate constant when Brownian coagulation occurs in the presence of size-dependent thermophoretic “drift”. Our approach, extends that of Simons [5], also avoiding the common approximation of “additive kernels” (see, e.g., Friedlander (2000) [6]). As in our recent paper (Rosner and Arias-Zugasti (2011) [7]), we are inevitably led to the remarkable need for a coagulation rate “constant” which not only depends on the local thermodynamic state of the carrier gas (via  $T$  and  $p$ ) but also on the magnitude of the local temperature gradient—a feature which transcends linear irreversible thermodynamics. The dynamics of thermophoretically-modified Brownian coagulation is analyzed by solving the corresponding nonlinear integro-PDE governing the evolution of the aerosol population size distribution in Sections IV and V. In particular, Section V outlines our use of both Gaussian quadrature-based “moment” methods (QMOM; McGraw (1997) [8]) and orthogonal collocation numerical methods (Arias-Zugasti [9, 10]). These methods are efficient enough to enable accurate “long-time” predictions of “quasi-self-preserving” (QSP-) populations, asymptotically reached in the long-time limit. Our principal assumptions are then briefly revisited and discussed in Section VI, which includes dimensionless criteria for precluding other potential complicating factors not considered here, such as : initial departures from the continuum (Stokes drag-) limit, simultaneous sedimentation, Marangoni-flow-induced mist droplet thermophoresis, finite-rate coalescence, and even dense (non-ideal) vapor effects. Section VII concludes this paper with the principal implications of our present methods and results, including mention of a method to allow additional sources of relative inter-particle drift (e.g., sedimentation, electrophoresis, ...)—generalizations which will necessary be left to follow-on studies.

## II. BASIC ASSUMPTIONS OF PRESENT MODEL

To identify and examine the characteristic new features of aerosol dynamics in the presence of simultaneous Brownian- and thermophoretic coagulation mechanisms, we deliberately exploit an idealized mathematical model based on the following simplifying assumptions ; viz. the evolving aerosol under study is assumed to be :

- A1. present at low volume fraction in a thermodynamically ideal carrier gas characterized by a mean-free-path ( $\ell$ ) small compared to the mean diameter (e.g., Sauter mean diameter (SMD)) of the population
- A2. comprised of spherical particles of a single substance which coalesce rapidly on the time-scale set by inter-particle binary encounters
- A3. comprised of particles acted upon by a (creep-driven) size-dependent force which causes them to drift down the local temperature gradient (as would an isolated solid of the same Fourier thermal conductivity in the same local gaseous environment)
- A4. not exchanging energy with the local gas or the local environment, resulting in the sol particle temperatures being close to the local gas temperature
- A5. describable by a continuous local droplet size distribution (DSD) of the form  $n(v, t)$  (in terms of particle volume  $v$  and time  $t$ ) satisfying a Smoluchowski- type integro-PDE in the absence of particle growth from the vapor phase, or the nucleation of new particles. Particle volume is assumed to be conserved upon each successful binary encounter

A6. not acted upon by additional forces capable of modifying the local coagulation rate (including gravitational- and electrostatic- body forces, ...) or the break-up of existing particles.

Explicit criteria sufficient to ensure the validity of most of these assumptions in any particular application will be presented and discussed in Section VI. For the present, however, we wish to identify and display (Section V) the expected features of coagulation under the simultaneous influence of Brownian motion and thermophoresis in an externally imposed gas temperature gradient. For example, even if only modest to begin with, will thermophoresis ultimately dominate the Brownian mechanism? Would novel quasi-self-preserving (QSP-) DSD “shapes” evolve showing the influence of thermophoresis? How “broad” will these populations be and how long will it take for approximate QSP behavior to set in? etc.

Of course, in practice we expect the onset of other complicating phenomena not considered here, which require future generalizations of the present model. For instance, the local environment will generally change with (residence-) time and additional coagulation mechanisms may set in (e.g., sedimentation when SMD exceeds a calculable threshold size (Section VIC), or fractal-like aggregate formation when the coalescence rate becomes too slow, etc.). In this regard, while some of these generalizations appear to be straightforward, as briefly outlined in Sections VI and VII, others will have to be left for necessary extensions of the present work.

### III. RATE CONSTANT FOR BROWNIAN COAGULATION IN PRESENCE OF THERMOPHORESIS

It is well known that, in the continuum regime, particles of different sizes finding themselves in a temperature gradient will experience different thermophoretic drift velocities [6, 11]. Therefore, this phenomenon can be responsible for collisions between particles of different sizes, which can lead to the subsequent coagulation (as recently shown by Rosner and Arias-Zugasti (2011) [4])—this occurs, for instance, for particles with different sedimentation velocities under the more familiar action of gravity. The rate constant for thermophoretically dominated coagulation adopted here is given by [4, 12]

$$\beta_{\text{TP},12} = \pi \cdot (a_1 + a_2)^2 \cdot \|\mathbf{V}_1 - \mathbf{V}_2\|, \quad (1)$$

where  $a_i$  and  $\mathbf{V}_i$  are the radius and the thermophoretically induced drift velocity of particle  $i$ . In terms of the dimensionless thermophoretic particle “diffusivity”, written here as:  $\tilde{\alpha} \equiv \alpha_T D / \nu$ , the vector expression for the particle drift velocity is given by

$$\mathbf{V}_i = \tilde{\alpha}_i \nu \cdot (-\nabla \ln T), \quad (2)$$

where  $T$  is the local carrier gas absolute temperature,  $\nu$  the carrier gas momentum diffusivity (i. e. the kinematic viscosity),  $D$  the Brownian diffusion coefficient, and  $\alpha_T$  (dimensionless) an effective thermal diffusion factor. For a spherical particle with intrinsic Fourier thermal conductivity  $k_p$  and diameter  $d_p$  the decisive factor  $\tilde{\alpha}$  depends on particle size (via the Knudsen number based on gas mean free path  $\ell$  and particle diameter:  $\text{Kn} \equiv \ell / d_p$ ) and thermal conductivity ratio  $k_p / k_g$  (where  $k_g$  is the gas thermal conductivity), via the simple semi-empirical relation [13]

$$\tilde{\alpha} = \frac{2C_s \cdot ((k_g / k_p) + 2C_t \text{Kn}) \cdot C}{(1 + 6C_m \text{Kn}) \cdot (1 + 2(k_g / k_p) + 4C_t \text{Kn})}, \quad (3)$$

where  $C$  is the Cunningham-Millikan Stokes drag correction factor,  $C_t$  is the gas/solid temperature jump coefficient, and  $C_m$  and  $C_s$  are the gas/solid momentum exchange and thermal slip coefficients respectively. The values of these gas/solid interaction coefficients [13] can be estimated from kinetic theory, approximate values are given after Eqs. (2.21 & 2.56) of [6].

On the other hand, the rate constant for the well known case of Brownian coagulation in the continuum regime, derived by Smoluchowski (see, e.g., [6]), is given by

$$\beta_{\text{B},12} = 4\pi \cdot (D_1 + D_2) \cdot (a_1 + a_2) \quad (4)$$

where the Brownian diffusion coefficient is

$$D = \frac{k_B T}{6\pi\mu a} \cdot C, \quad (5)$$

where  $\mu$  is the gas shear viscosity,  $k_B$  is the Boltzmann constant and the remaining symbols have already been defined.

Although the assumption of rate law additivity for different coagulation processes is usual in the literature, a more accurate approximation has been adopted in the present work. In this regard, the rate constant for combined

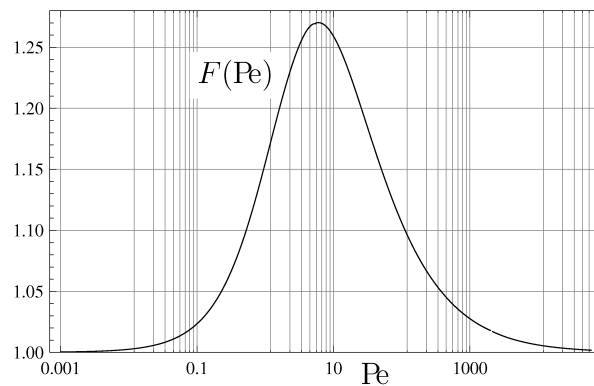


FIGURE 1. Factor  $F(\text{Pe})$  vs.  $\text{Pe}$ , from Eq. (7) [5].

Brownian + thermophoretic coagulation has been obtained following the classical Smoluchowski formulation [6], based on the calculation of the diffusive flow towards a target particle, but including an additional convective term which accounts for the relative thermophoretic speed between the particles. Assuming that all collisions lead to the corresponding coagulation (i.e. neglecting collision efficiency corrections) and assuming a rectilinear thermophoretic drift superimposed with the Brownian motion (i.e. neglecting hydrodynamic creep-flow interactions between the particles), the convective-diffusion equation that determines the coagulation rate is the same as the one considered by Simons et al. [5] for the combined Brownian + differential sedimentation coagulation case, exchanging their sedimentation velocities by the corresponding thermophoretic velocities. Hence, the combined coagulation rate is given by

$$\beta_{12} = (\beta_{\text{B},12} + \beta_{\text{TP},12}) \cdot F(\text{Pe}_{12}) \quad (6)$$

where the correction factor  $F(\text{Pe})$  is given by [5]

$$F(\text{Pe}) = \frac{4\pi/\text{Pe}}{4 + \text{Pe}} \sum_{n=0}^{\infty} (-1)^n (2n + 1) \frac{I_{n+1/2}(\text{Pe}/2)}{K_{n+1/2}(\text{Pe}/2)} \quad (7)$$

with  $I$  and  $K$  being the modified Bessel functions and  $\text{Pe}$  the Peclet number, defined as the ratio between the relative thermophoretic and Brownian diffusion velocities

$$\text{Pe}_{12} = \frac{\|\mathbf{V}_1 - \mathbf{V}_2\|}{(D_1 + D_2)/(a_1 + a_2)}. \quad (8)$$

Owing to the low convergence rate of the series in Eq. (7) and the extremely large numbers involved when the Peclet number becomes large, the accurate numerical evaluation of Eq. (7) for large values of  $\text{Pe}$  is a mathematically involved and time-consuming task [14]. In this regard, the convenient approximate least-squares formula provided by [15] has been used for our present calculations.

The time evolution of an initially lognormal DSD under the combined kernel Eq. (6) has been analyzed and is shown below (section V) as a function of the *reference* Peclet number  $\text{Pe}_{\text{ref}}$ , defined as the ratio between the characteristic evolution times for the initial DSD function under the Brownian and thermophoretically dominated coagulation kernels acting alone

$$\text{Pe}_{\text{ref}} \equiv \frac{t_{\text{B,ref}}}{t_{\text{TP,ref}}}. \quad (9)$$

These characteristic evolution times are given (in terms of the unconditional particle number density in the initial population  $N_0$ ) by  $t_{i,\text{ref}} \equiv 1/(\beta_{i,\text{ref}}N_0)$ . Thus

$$t_{\text{B,ref}} = \frac{3\mu}{8k_B T N_0}, \quad \text{and} \quad t_{\text{TP,ref}} = \frac{4}{\pi d_{\text{ref}}^2 V_{\text{ref}} N_0}, \quad (10)$$

where the reference particle diameter  $d_{\text{ref}}$  is defined as the Sauter mean diameter of the initial population (SMD), and where the reference velocity  $V_{\text{ref}}$  is the thermophoretic drift velocity of a SMD droplet in the limit  $k_p/k_g = \infty$ .

As a consequence, the combined coagulation kernel is finally written as

$$\beta_{12} = \beta_{\text{B,ref}} (K_{\text{B},12} + \text{Pe}_{\text{ref}} K_{\text{TP},12}) \cdot F(\text{Pe}_{12}) \quad (11)$$

where the dimensionless coagulation kernels  $K_{\text{B},12}$  and  $K_{\text{TP},12}$  are defined by  $K_{i,12} \equiv \beta_{i,12}/\beta_{i,\text{ref}}$  and  $\text{Pe}_{\text{ref}}$  (Eq. (9)) plays the role of an independent parameter that measures the relative importance of both coagulation processes in the initial population. Namely, according to the former definition of  $\text{Pe}_{\text{ref}}$  (Eq. (9)) we find that the reference Peclet number is related to the prevailing conditions in the initial population by

$$\text{Pe}_{\text{ref}} = \frac{\tilde{\alpha}_{\infty,\text{ref}}}{32\text{Kn}_{\text{ref}}} \cdot \text{Sc}_{\text{ref}} \cdot \|\nabla \ln T\| \ell \quad (12)$$

where subscript ref corresponds to a SMD particle in the initial population, subscript  $\infty$  corresponds to the limit  $k_p/k_g = \infty$  and  $\text{Sc} = \nu/D$  is the corresponding particle Schmidt number. It may be easily seen that the first factor  $\tilde{\alpha}_{\infty,\text{ref}}/32\text{Kn}_{\text{ref}}$  reaches a constant value close to 0.32 for  $\text{Kn}_{\text{ref}} < 10^{-2}$ .

#### IV. POPULATION BALANCE EQ. GOVERNING CONTINUOUS DSD-FUNCTION

Once the coagulation rate law  $\beta_{12}$  is known in terms of the particle state variables (Eq. (11)), the population balance equation that determines the evolution of an initial particle distribution is the Smoluchowski coagulation equation [6]

$$\frac{\partial n}{\partial t} = \mathcal{B} - \mathcal{D}, \quad (13)$$

where the particle *production* ( $\mathcal{B}$ ) and *destruction* ( $\mathcal{D}$ ) terms by coagulation are explicitly given by

$$\begin{aligned} \mathcal{B}(v) &= \frac{1}{2} \int_0^v dv' \beta(v', v-v') n(v') n(v-v') \\ \mathcal{D}(v) &= n(v) \int_0^\infty dv' \beta(v, v') n(v') \end{aligned} \quad (14)$$

in terms of particle volume  $v = (4\pi/3)a^3$ .

A systematic parametric study of this integro-PDE has been performed using a two-stage combined quadrature method of moments (QMOM [8]) and orthogonal collocation method [16], as reported below. The values for the reference Peclet number considered in the numerical calculations shown below go from  $\text{Pe}_{\text{ref}} = 10^{-3}$  (corresponding to coagulation dominated by Brownian motion) to  $\text{Pe}_{\text{ref}} = 10^3$  (corresponding to thermophoretically dominated coagulation). Regarding the Fourier thermal conductivity ratio  $k_p/k_g$ , the values considered were 10,  $10^2$ ,  $10^3$ ,  $10^4$  and  $\infty$ . In all the cases the asymptotic results for pure Brownian ( $\text{Pe}_{\text{ref}} = 0$ ) and pure thermophoretic ( $\text{Pe}_{\text{ref}} = \infty$ ) coagulation are also shown for reference (gray lines). The results from QMOM are shown as a function of the reference Peclet number in Figs. 2, 3 and 4. On the other hand, the results from orthogonal collocation are presented in Fig. 5.

##### A. Numerical Integration Based on QMOM

In the first stage, the time evolution of the  $2N$  lowest order moments of the DSD  $n(v, t)$

$$\mu_k(t) \equiv \int_0^\infty dv v^k n(v, t), \quad N = 0, 1, 2, \dots, 2N - 1 \quad (15)$$

has been computed by means of QMOM [8], solving the corresponding evolution equations, given by [17]

$$\begin{aligned} \frac{d\mu_k}{dt} &= \frac{1}{2} \int_0^\infty dv' \int_0^\infty dv'' \beta(v', v'') n(v') n(v'') \\ &\cdot \left[ (v' + v'')^k - v'^k - v''^k \right], \quad k = 0, \dots, 2N - 1. \end{aligned} \quad (16)$$

Although QMOM calculations based on a relatively low number of quadrature abscissae are usual in the literature (for instance  $N \simeq 3$ ), in the present case a higher number of abscissae were needed to reach convergence for intermediate values of the reference Peclet number. Thus, in the present work  $N = 6$  quadrature abscissae were used in all the QMOM calculations.

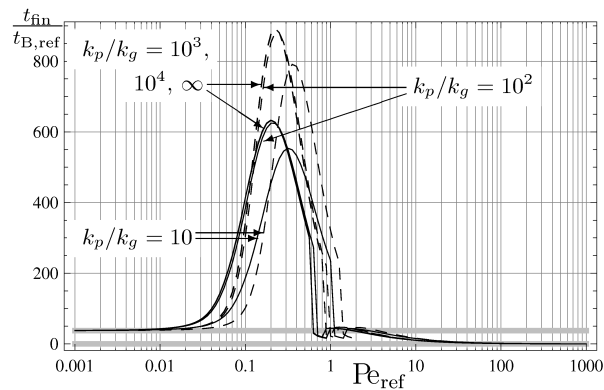


FIGURE 2. Time needed to approach the self-preserving DSD function vs.  $\text{Pe}_{\text{ref}}$  for several values of  $k_p/k_g$ . The solid lines correspond to the coagulation frequency given by Eq. (6), the broken lines correspond to Eq. (6) assuming  $F(\text{Pe}) = 1$ . The horizontal gray lines correspond to the asymptotic results of pure Brownian ( $\text{Pe}_{\text{ref}} = 0$ ) and pure thermophoretic ( $\text{Pe}_{\text{ref}} = \infty$ ) coagulation.

The QMOM-based time integration of Eq. (13) was carried until the self-preserving size distribution function was reached to within a certain tolerance. As is well known, in the long-time limit coagulation-aged size distribution functions approach (in general) a self-similar form  $\psi(\eta)$  [6, 18]; i.e., if  $\psi(\eta, t)$  is defined according to

$$n(v, t) \equiv N \psi(v/\bar{v}, t)/\bar{v}, \quad (17)$$

(where  $N = \mu_0(t)$  is the unconditional droplet number density,  $\bar{v}(t) = \mu_1(t)/\mu_0(t)$  is the time-dependent average particle volume, and  $\eta \equiv v/\bar{v}$  is the similarity variable), we find that in the long-time limit  $\psi(\eta, t)$  approaches a function that does not depend on time. According to the former definition (Eq. (17)), the moments of  $\psi(\eta, t)$  ( $\mu_k^\psi$ ) are dimensionless and fulfill  $\mu_0^\psi = \mu_1^\psi = 1$ , and are related to the moments of  $n(v, t)$  by  $\mu_k^\psi = (\mu_k/\mu_0)/\bar{v}^k$ , as can be easily seen.

If the DSD approaches a self-similar form in the long-time limit, then  $\psi(\eta, t)$  becomes independent of time for long times, and as a consequence all its moments should reach constant values in the limit  $t \rightarrow \infty$ . Based on this expected behavior of  $\psi(\eta, t)$ , the condition used in the present calculations to test whether the self-preserving size distribution function has been reached, is determined by the variation rate of the 5 lowest order moments of  $\psi(\eta, t)$ . This condition is given by :

$$\frac{t_{\text{B,ref}}}{(1 + \text{Pe}_{\text{ref}}) \cdot F(\text{Pe}_{\text{ref}})} \sum_{k=0}^4 \left| \frac{d\mu_k^\psi}{dt} \right| < \varepsilon. \quad (18)$$

The numerical solution of Eq. (16) by means of QMOM has been calculated for  $\varepsilon$  between  $10^{-1}$  and  $10^{-3}$ . In this respect it was found that the principal effect of changing the value of  $\varepsilon$ , in that range, was simply to re-scale the times at which the self-preserving size distribution is “reached” (obviously this time approaches infinity as  $\varepsilon \rightarrow 0$ , since the approach is asymptotic). Besides the re-scaling of the time needed to reach self-preservation no qualitative changes were observed (with  $\varepsilon$  in the aforementioned range), and no significant quantitative changes were observed for  $\varepsilon < 10^{-2}$ . Thus, a tolerance  $\varepsilon = 10^{-2}$  was finally chosen for the results presented here.

The QMOM-based solution of Eq. (16) provides information on the time evolution of the considered moment set ( $\mu_k$ , with  $k = 0, 1, \dots, 2N - 1$ ), and by means of the condition Eq. (18) it also provides information on the time needed to approach the self-preserving size distribution function  $\psi(\eta)$  to within a certain tolerance.

It has been found that the present self-similarity test (Eq. 18) leads to characteristic times for reaching the self-preserving form that are about an order of magnitude longer than most self-preservation times reported in the literature [19], which are based only on the standard deviation of the self-preserving size distribution function. However, our results show that *even though the standard deviation of  $\psi(\eta, t)$  reaches its asymptotic value relatively fast, one must wait longer times for the higher order moments.*

The results for the time ( $t_{\text{fin}}$ ) needed to reach the self-preserving form (according to (Eq. 18)) are shown in Fig. 2 for both, the simple addition kernel (assuming  $F(\text{Pe}) = 1$ , broken lines), and the more accurate combined kernel (Eq. (6) with  $F(\text{Pe})$  given by Eq. (7), solid lines). The results for the lowest order moments of  $\psi(\eta) \equiv \psi(\eta, t_{\text{fin}})$  are shown in Fig. 3 in terms of the geometric standard deviation, the (asymmetry parameter) skewness and the (flatness

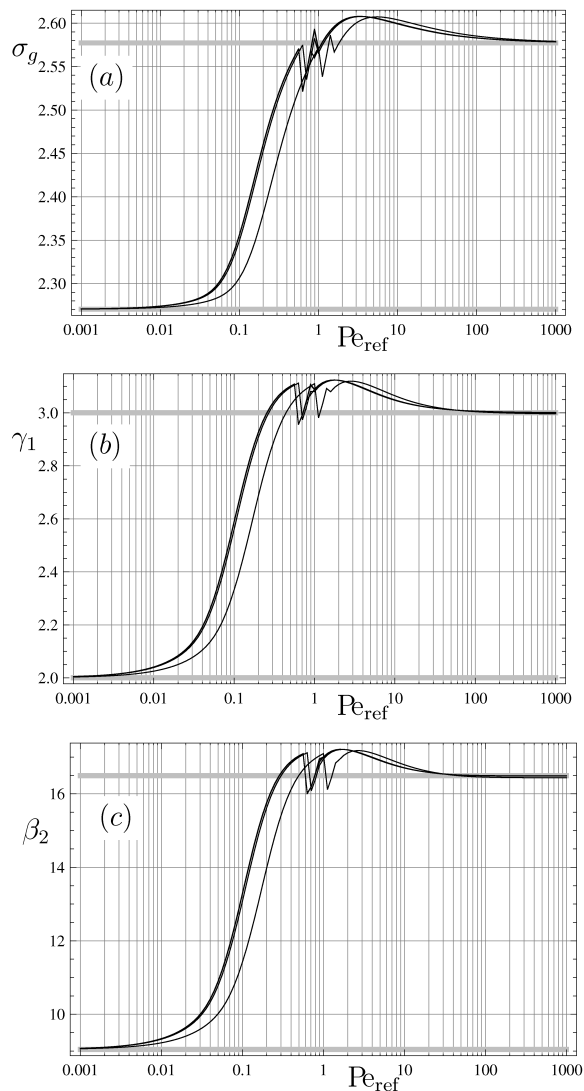


FIGURE 3. Moments of the self-preserving size distribution function as a function  $\text{Pe}_{\text{ref}}$  for  $k_p/k_g = 10$  (separate lines),  $10^2$ ,  $10^3$ ,  $10^4$  and  $\infty$  (almost superimposed lines). Top (a) : geometric standard deviation  $\sigma_g$ , center (b) skewness  $\gamma_1$ , bottom (c) kurtosis  $\beta_2$ . The horizontal gray lines correspond to the asymptotic results of pure Brownian ( $\text{Pe}_{\text{ref}} = 0$ ) and pure thermophoretic ( $\text{Pe}_{\text{ref}} = \infty$ ) coagulation.

parameter) kurtosis. In Fig. 4 we show the ratio between the skewness and kurtosis of  $\psi(\eta)$  and the corresponding results found for a lognormal fit of  $\psi(\eta)$ .

One of the goals of the present work is to test (in the case of Brownian + thermophoretic coagulation) the frequently used simplification of assuming an *addition* collision frequency when several coagulation processes take place simultaneously. In this regard, our results show significant differences (close to 30%) in the time needed to reach self-preservation when both coagulation mechanisms are equally important, i.e., for intermediate values of the reference Peclet number (see Fig. 2). As expected, these differences become insignificant as either asymptote,  $\text{Pe}_{\text{ref}} \rightarrow 0$  or  $\text{Pe}_{\text{ref}} \rightarrow \infty$ , is approached. On the other hand, the differences between the simple addition kernel and the combined coagulation kernel regarding the moments of the final self-similar distribution  $\psi(\eta)$  were only about 10%, and as a consequence only the results corresponding to the coagulation kernel given by Eq. (6) with  $F(\text{Pe})$  given by Eq. (7) have been plotted for clarity.

Regarding the dependence of the coagulation dynamics on the particle/gas thermal conductivity ratio ( $k_p/k_g$ ), our results show that, in the range considered here ( $k_p/k_g > 10$ ), this dependence becomes negligible as either asymptote ( $\text{Pe}_{\text{ref}} \rightarrow 0$  or  $\text{Pe}_{\text{ref}} \rightarrow \infty$ ) is approached. On the other hand, for intermediate values of the reference Peclet number this dependence is appreciable only in the limit of low particle thermal conductivity (i. e. when  $k_p/k_g$  approaches 10), but becomes negligible for  $k_p/k_g > 10^2$  for all values of  $\text{Pe}_{\text{ref}}$ . Of course it was expected that the results should become

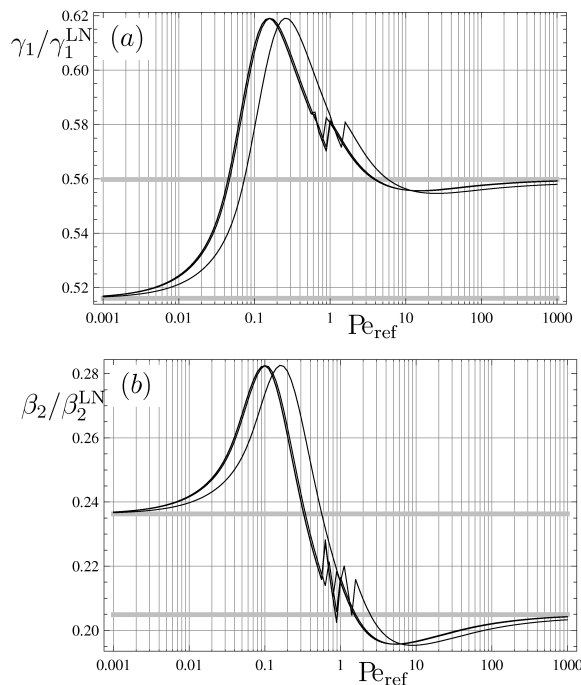


FIGURE 4. Moments of the self-preserving size distribution function over the corresponding moments of  $\psi(\eta)$  fitted to a log-normal distribution, as a function  $\text{Pe}_{\text{ref}}$  for  $k_p/k_g = 10$  (separate lines),  $10^2$ ,  $10^3$ ,  $10^4$  and  $\infty$  (almost superimposed lines). Top (a) : skewness  $\gamma_1$ , bottom (b) kurtosis  $\beta_2$ . The horizontal gray lines correspond to the asymptotic results of pure Brownian ( $\text{Pe}_{\text{ref}} = 0$ ) and pure thermophoretic ( $\text{Pe}_{\text{ref}} = \infty$ ) coagulation.

independent of the  $k_p/k_g$  ratio in the small  $\text{Pe}_{\text{ref}}$  limit (i. e. as the pure Brownian coagulation limit is approached), but it is remarkable that the results become also independent of  $k_p/k_g$  in the opposite limit (corresponding to pure thermophoretic coagulation).

This result can be easily explained in the following way. Assuming that the diameters of the colliding particles fulfill  $d_1, d_2 \gg \ell$ , which certainly holds in the long time limit, to leading order in  $\ell/d_i$  the coagulation frequency Eq. (6) is given by

$$\frac{\beta_{12}}{\beta_{\text{B,ref}}} \simeq \frac{(d_1 + d_2)^2}{4d_1d_2} \left( 1 + \frac{4\text{Pe}_{\text{ref}}}{1 + 2(k_g/k_p)} \cdot \left| \frac{d_1}{d_{\text{ref}}} - \frac{d_2}{d_{\text{ref}}} \right| \right) \cdot F(\text{Pe}_{12}). \quad (19)$$

Hence, in the limit  $\text{Pe}_{\text{ref}} \gg 1$  the thermophoretic part dominates, and in that case the dependence in  $k_p/k_g$  is given only by the factors  $(1 + 2k_g/k_p)^{-1}$  and  $F(\text{Pe}_{12})$ . The latter factor depends also in  $k_p/k_g$  since, in the limit  $d_1, d_2 \gg \ell$ , the Peclet number  $\text{Pe}_{12}$  is given by

$$\text{Pe}_{12} \simeq \frac{16\text{Pe}_{\text{ref}}}{1 + 2(k_g/k_p)} \left| \frac{d_1}{d_{\text{ref}}} - \frac{d_2}{d_{\text{ref}}} \right| \quad (20)$$

to leading order in  $\ell/d_i$ . Therefore, if  $\text{Pe}_{\text{ref}} \gg 1$ , in the long-time limit the dependence of  $\beta_{12}$  (Eq. (19)) on  $k_p/k_g$  given by the factor  $(1 + 2k_g/k_p)^{-1}$  affects only the time scale, but not the final self-preserving distribution reached. On the other hand, the dependence on  $k_p/k_g$  given by the factor  $F(\text{Pe}_{12})$  (Eq. (20)) affects only the length scale (defining an “effective” reference diameter as  $d_{\text{ref,eff}} \equiv [1 + 2(k_g/k_p)] d_{\text{ref}}$ ), but not the final distribution reached.

Hence, as a consequence of these approximate symmetry relations of the combined coagulation kernel reached in the long-time limit (i. e. for  $d_1, d_2 \gg \ell$ ), the results for  $\psi(\eta)$  become independent of  $k_p/k_g$ , not only in the small  $\text{Pe}_{\text{ref}}$  limit (as expected), but also in the opposite limit  $\text{Pe}_{\text{ref}} \gg 1$ , corresponding to coagulation dominated by thermophoresis.

On the other hand, if we consider intermediate values of the reference Peclet number, in the range of values of  $k_p/k_g$  considered here ( $k_p/k_g > 10$ ) we find that, for  $k_p/k_g = 10^2$  or larger the former coagulation kernel differs only in a small correction (of order  $10^{-2}$  or smaller) from the coagulation frequency corresponding to  $k_p/k_g = \infty$ . As a

consequence, the dependence on  $k_p/k_g$  is only appreciable for intermediate values of  $\text{Pe}_{\text{ref}}$  in the limit of low particle/gas thermal conductivity ratio (i. e. for  $k_p/k_g \simeq 10$ ), being almost negligible for  $k_p/k_g = 10^2$  or larger. In particular, for  $k_p/k_g = 10^3$  or larger our numerical results become totally indistinguishable from the results corresponding to the limit  $k_p/k_g = \infty$  (see Figs. 2, 3, 4 and 5).

Regarding the time needed to reach self-preservation ( $t_{\text{fin}}$ ), figure 2 shows a dramatic increase in  $t_{\text{fin}}$  for intermediate values of the reference Peclet number, whereas the much shorter self-preservation times corresponding to pure Brownian and thermophoretic coagulation are recovered for  $\text{Pe}_{\text{ref}} < 10^{-2}$  and  $\text{Pe}_{\text{ref}} > 10$  respectively. This result will be explained in Section V, along with the results found for the function  $\psi(\eta)$ , computed using orthogonal collocation (see also section IV B below).

Finally, regarding the shape of the self-preserving DSD function  $\psi(\eta)$ , our results (Fig. 4) show that  $\psi(\eta)$  is not a log-normal distribution, irrespective of the reference Peclet number and the thermal conductivity ratio. As a consequence, the approximation of considering a closed form mathematical form for the DSD (log-normal in this case), which is a frequently used approximation, is not justified, and may be misleading, yielding increasing errors as higher order moments of the DSD are considered.

## B. Numerical Integration Based on Orthogonal Collocation

While QMOM is extremely efficient, it has the limitation that it only provides information about the *moments* (Eq. (15)) of the number density distribution function, which remains an unknown function. To calculate the evolution of the number density  $n(v, t)$ , from its initial condition until the self-preserving form is reached, one needs to integrate Eq. (13). But then, since one needs to carry this time integration until relatively long times, one is forced to discretize extensive regions of the state variables space (here particle volume), because the average particle volume and standard deviation of a population  $n(v, t)$  under coagulation increase with time. As a consequence, if a time-independent discretization is used, this would force us to consider extremely fine discretizations, resulting in a computationally expensive scheme. On the other hand, a time-dependent discretization that evolves in time in an adaptive way, determined by the time evolution of  $n(v, t)$ , can produce an efficient numerical method that enables the time integration of Eq. (13) for long times.

In principle there are several possible ways of implementing adaptive spectral schemes to solve Eq. (13). On one hand one can compute a time-dependent spectral basis, which is specially suited to solve Eq. (13), and then use this basis to perform the spectral expansion of  $n(v, t)$ , as successfully implemented in [20, 21]. Another possibility is to introduce a time-dependent mapping based on the time evolution of  $n(v, t)$ , in such a way that the region  $v \in [v_{\text{min}}, v_{\text{max}}]$ , where  $n(v, t)$  is mainly located, is mapped to the standard interval  $[-1, 1]$ , and then perform a spectral expansion of  $n(v, t)$  in terms of a complete basis on that interval (for instance Chebyshev or Legendre), as successfully implemented in [22, 23]. The numerical method used here belongs to this second class of adaptive schemes. In the present calculations Eq. (13) has been numerically integrated using orthogonal collocation in terms of an adaptive variable  $x$ , defined as the ratio between particle volume  $v$  and the time-dependent standard deviation of  $n(v, t)$  ( $\sigma(t)$ ), computed previously using QMOM. Hence, in terms of the mapped variable  $x$  the standard deviation of  $n(x, t)$  is always 1, and a time-independent accurate discretization in terms of  $x$  allows for an efficient numerical solution of Eq. (13). This numerical integration of Eq. (13) has been carried out for values of  $t$  between 0 and the  $t_{\text{fin}}$  previously derived from QMOM.

The numerical method used here to integrate Eq. (13), written in terms of the mapped variable  $x \equiv v/\sigma(t)$ , has been orthogonal collocation [16]. The spectral basis used was the truncated Whitaker cardinal basis [16], with 75 spectral components. Since orthogonal collocation involves the evaluation of the differential equation at the corresponding collocation abscissae ( $x_i$ ), which are constant in time, when this method is implemented in terms of the mapped variable  $x$  we find that the coagulation term has to be evaluated at the time-dependent locations  $v_i(t) = x_i\sigma(t)$ . Hence, in principle this strategy would result in a quite expensive numerical scheme, since all the integrals that appear in the coagulation term of Eq. (13) would have to be recalculated at every time step. However, by means of the *fast algorithm* introduced in Ref. [9] this problem can be avoided, which results in an extremely efficient numerical method. This strategy has also been successfully used in [4, 7]. More details on the implementation of orthogonal collocation in terms of the mapped variable  $x \equiv v/\sigma(t)$ , for aerosol dynamics under coagulation, can be found in [10].

The results for the self-preserving normalized size distribution function reached in the long time limit  $\psi(\eta)$ , found according to the self-similarity test Eq. (18), are shown in Fig. 5 as a function of the reference Peclet number (see solid lines), together with the results corresponding to pure Brownian and pure thermophoretic coagulation (see thick gray lines). As may be seen in Fig. 5, for  $\text{Pe}_{\text{ref}} < 10^{-2}$  the quasi-self-preserving size distribution function is almost identical to the self-preserving size distribution function corresponding to pure Brownian coagulation. On the other hand, for  $\text{Pe}_{\text{ref}} > 10$  the quasi-self-preserving size distribution function is almost identical to the result found for pure thermophoretic coagulation.

As can be seen in Fig. 5, both asymptotic limits  $\text{Pe}_{\text{ref}} \rightarrow 0$  and  $\text{Pe}_{\text{ref}} \rightarrow \infty$  lead to self-preserving size distribution

functions which do not depend on the thermal conductivity ratio ( $k_p/k_g$ ), as could be expected (see Section IV A). On the other hand, for intermediate values of the reference Peclet number, and for values of  $k_p/k_g$  in the range considered, the dependence of  $\psi(\eta)$  on  $k_p/k_g$  is almost negligible. According to our numerical results  $\psi(\eta)$  becomes slightly dependent on  $k_p/k_g$  only for the intermediate values of  $\text{Pe}_{\text{ref}}$  between 0.1 and 1, where the self-preserving size distribution function corresponding to  $k_p/k_g = 10$  can be slightly distinguished from the self-preserving size distribution functions found for  $k_p/k_g = 10^2, 10^3, 10^4$  and  $\infty$ , which are totally superimposed. The results for  $\psi(\eta)$  corresponding to  $\text{Pe}_{\text{ref}} < 0.1$  or  $\text{Pe}_{\text{ref}} \geq 1$  are totally independent of  $k_p/k_g$ . The reason of this near in-dependence of  $\psi(\eta)$  on the particle/gas thermal conductivity ratio has already been explained in Section IV A.

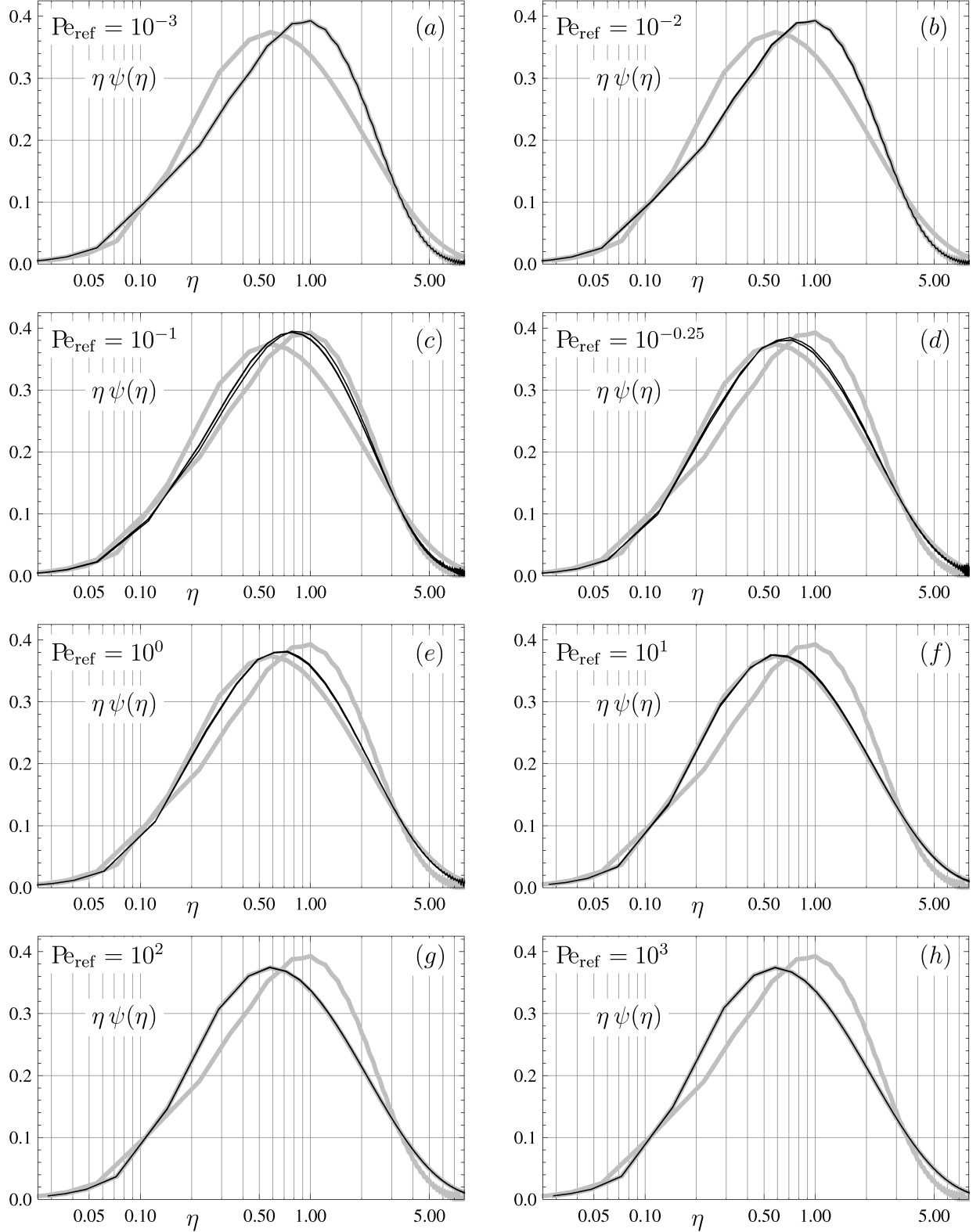


FIGURE 5. Solid lines : normalized self-preserving DSD functions reached in the long time limit for several values of  $\text{Pe}_{\text{ref}}$  and  $k_p/k_g = 10, 10^2, 10^3, 10^4$  and  $\infty$ . The gray lines correspond to pure Brownian ( $\text{Pe}_{\text{ref}} = 0$ ) and pure thermophoretic ( $\text{Pe}_{\text{ref}} = \infty$ ) coagulation. The results for different values of  $k_p/k_g$  are almost superimposed for all values of  $\text{Pe}_{\text{ref}}$ , except for  $\text{Pe}_{\text{ref}} = 10^{-1}$  and  $10^{-0.25}$  (see (c) and (d)) where  $\psi(\eta)$  corresponding to  $k_p/k_g = 10$  can be distinguished from the remaining values. For all values of  $k_p/k_g$ ,  $\psi(\eta)$  becomes indistinguishable from the pure Brownian coagulation QSP DSD for  $\text{Pe}_{\text{ref}} \leq 10^{-2}$  (see (a) and (b)), and from the pure thermophoretic coagulation QSP DSD for  $\text{Pe}_{\text{ref}} \geq 10^1$  (see (f), (g) and (h)).

## V. QMOM/OC-RESULTS FOR DSD-EVOLUTION ; ULTIMATE TP-DOMINANCE ?

The results for  $\psi(\eta)$  computed using orthogonal collocation show a smooth transition from the pure Brownian coagulation limit (reached for  $\text{Pe}_{\text{ref}} \leq 10^{-2}$ ) to the pure thermophoretic coagulation limit (reached for  $\text{Pe}_{\text{ref}} \geq 10$ ), see Fig. 5. As already mentioned these results are almost independent of  $k_p/k_g$  (Section IV A). However, even though this smooth transition from pure Brownian to pure thermophoretic coagulation, as a function of  $\text{Pe}_{\text{ref}}$ , seems a natural result, a different result could have been expected according to the combined Brownian + thermophoretic coagulation frequency given by Eq. (6), as explained below.

For arbitrary long times the characteristic sizes of the colliding particles are expected to become very large compared to the reference size, which is based on the initial size distribution function. Likewise, the typical difference in diameter between two colliding particles is expected to become very large compared to the reference diameter. Hence, in the long time limit the coagulation frequency given by Eq. (6) approaches the corresponding limit for  $d_1, d_2 \gg \ell$ , which is given by Eq. (19) and Eq. (20). As a consequence, as long as  $\text{Pe}_{\text{ref}} > 0$ , at sufficiently long times the thermophoretic contribution becomes dominant over the Brownian contribution, i.e. thermophoretic coagulation (if present) ultimately dominates over Brownian coagulation for arbitrary long times irrespective of  $\text{Pe}_{\text{ref}}$ .

The reason why this behavior is not observed in our numerical integration of Eq. (13) is because for small values of the reference Peclet number the stopping-test condition (Eq. (18)) is satisfied before the thermophoretic contribution becomes relevant. This is because the characteristic evolution time of the aerosol scales with the inverse of the unconditional particle number density  $N(t)$ , becoming very large in the long time limit as  $N(t)$  decreases. As a consequence, even though no true self-similar behavior may have been reached yet, the stopping-test condition Eq. (18) becomes eventually fulfilled in the long time limit.

This explains the extraordinarily long times needed to reach “quasi”-self preservation for intermediate values of the reference Peclet number (Fig. 2). When both (Brownian and thermophoretic) contributions to the coagulation frequency are relevant, the coagulation kernel is not a homogeneous function of particle size, and no true self-similar behavior is observed. However, for times long enough the characteristic coagulation time is so long that the coagulation process becomes slow enough for the stopping-test condition (Eq. (18)) to become satisfied, even though the DSD has not yet reached the asymptotic self-similar form.

This also explains the smooth transition found for  $\psi(\eta)$  between the pure Brownian and thermophoretic self-preserving functions. For  $\text{Pe}_{\text{ref}} < 10^{-1}$  long before the thermophoretic contribution becomes important the self-similar stopping test defined by Eq. (18) is fulfilled, yielding a self-similar distribution which is very close to the one corresponding to pure Brownian coagulation. On the other hand, for values of the reference Peclet number of order unity or larger, the thermophoretic contribution to the coagulation frequency is important right from the start. In these cases the self-similar distribution found is very close to the one corresponding to pure thermophoretic coagulation. In this respect, we recall [4] that in the long time limit the coagulation frequency corresponding to pure thermophoretic coagulation becomes a homogeneous function of degree 1 in particle diameter (degree 1/3 in particle volume). A similar conclusion can be drawn from Eq. (19) for the combined Brownian + thermophoretic coagulation considered here. However, for intermediate values of the reference Peclet number (for  $10^{-1} < \text{Pe}_{\text{ref}} < 1$  according to Fig. 2), both contributions to the coagulation frequency are equally important, which results in a coagulation frequency that is not a homogeneous function of particle size. For reference Peclet numbers close to 1 the contribution of the thermophoretic term becomes dominant before the stopping-test condition is fulfilled simply because of the decrease in  $N(t)$ , producing a dramatic reduction in  $t_{\text{fin}}$ , along with a rather fast transition in  $\psi(\eta)$  towards a function that is very close to the asymptotic self-similar distribution corresponding to pure thermophoretic coagulation.

In order to be observed in nature a coagulation-aged self-similar distribution should be reached in a reasonable time, before other processes (or changes in the environment) set in. In the case under consideration, for small values of the reference Peclet number the typical particle size needed for the thermophoretic contribution to become dominant over the Brownian contribution becomes extremely large. This has two consequences, on one hand it is possible that before this ultimate thermophoresis dominance may be observed other coagulation processes (i.e. sedimentation) may become important. On the other hand, since the characteristic coagulation time scales with the inverse of the total number density of the aerosol  $N(t)$  which decreases with time, if  $\text{Pe}_{\text{ref}}$  is too small the time needed before the ultimate thermophoresis dominance can be observed may become too large to be physically relevant.

As a consequence, even though in principle thermophoretic coagulation ultimately dominates over Brownian coagulation irrespective of  $\text{Pe}_{\text{ref}}$  (provided that  $\text{Pe}_{\text{ref}} > 0$ ), this result will only be observed for values of the reference Peclet number close to unity or larger, and for this reason the smooth transition between the pure Brownian and the pure thermophoretic self-similar distributions shown in Fig. 5 seems physically relevant.

## VI. DISCUSSION

### A. Collision Efficiency and Finite-Rate Coalescence

Our present results pertain to the limiting case that each binary encounter between particles of volumes  $v_1$  and  $v_2$  leads to “successful” coalescence, producing a spherical particle of volume  $v_1 + v_2$  before the next encounter with another particle. In the language of cloud physics we are assuming “unit collision efficiency (fraction)” —as is appropriate for collisions for which the average relative kinetic energy is insignificant compared to typical droplet surface energies (i.e. negligible Weber number).

Whether surface tension-driven viscous flow leads to coalescence on the coagulation time scale  $(\beta_{\text{ref}} N_p)^{-1}$  depends on a reference characteristic time estimated from :

$$t_{\text{coalesce}} = \pi \mu_L \frac{\text{SMD}}{\gamma_L} \quad (21)$$

where  $\gamma_L$  is the prevailing surface tension and  $\mu_L$  the dynamic viscosity (see, e.g. [6]). It is interesting to note that on this basis a micron-diameter molten iron micro-droplet near  $T_{mp} = 1808$  K would have a coalescence time of only 8.5 ns. Based on  $\beta_{\text{ref}} = (8/3)k_B T / \mu_g$ , appropriate for continuum regime Brownian coagulation, this would be insignificant compared to the coagulation time (of order 10 ms) of any such low volume fraction “mist” in, say, 1808 K helium (for which  $\mu_g = 0.62 \times 10^{-4}$  Pa s).

For sols comprised of more viscous liquids, or coagulation sufficiently far below the effective melting temperature, then “aggregation” would set in, leading to fractal-like “particle” morphologies [6] governed by rather different laws of diffusion and thermophoresis (e.g., Filippov et al. (2000) [24]).

### B. Marangoni-Induced Thermo-Phoresis

Our use of “solid body” thermophoresis results for micro-droplet transport in a temperature gradient requires further discussion. This is because there are situations where micro-flows driven by surface tension gradients can retard (or even reverse) the motion of micro-droplets in such environments.

For present purposes we merely envision an engineering environment in which such liquid/vapor interfaces are “contaminated”, retarding any surface tension gradient-driven flows. It should also be mentioned that the use of gas/liquid experimental results (e.g. oil droplet drag in low density gases) to describe gas/solid situations is common in aerosol science and technology, where contaminated liquid surfaces are avoidable only if extraordinary precautions are taken.

For some systems the aforementioned Marangoni-effect may be precluded simply based on the following “sufficient” condition :

$$\frac{\gamma_L}{d} < \left( \frac{T_c}{T} - 1 \right) (\text{Kn})^2 \cdot p \quad (22)$$

where  $p$  is the prevailing pressure and the Knudsen number  $\text{Kn} = \ell/d$  is necessarily  $\ll 1$  for the “continuum limit”. This can be derived by insisting that the difference in surface tension induced stress across the non-isothermal drifting droplet be small compared to the average Stokes drag stress. However, for many systems of practical interest this criterion would *not* be satisfied in the absence of surface contamination.

The consequences of Marangoni-driven flows are therefore certainly of theoretical interest—including the limiting case in which this is the dominant source of thermophoresis (from cold to hot). However, such extensions are beyond the scope of our present model, which can be regarded as applying to situations for which the viscosity ratio :  $\mu_L/\mu_g$  is large (say  $\mathcal{O}(10) \sim \mathcal{O}(1000)$ , but not “too large” (cf. the effect of  $\mu_L$  on the coalescence time, Eq. (21)).

### C. Body-Force “Sedimentation”

In the presence of a body force  $g$  (per unit mass) a particle of diameter  $d$  ( $d \gg \ell$ ) will sediment at the speed  $gt_p$ , where  $t_p$  is the familiar characteristic Stokes “stopping time”  $(1/18)\rho_p d_p^2/\mu_g$ . This implies that the velocity difference appearing in the corresponding coagulation rate constant will be proportional to  $|d_1^2 - d_2^2|$  for a common  $\rho_p$  value. When one then examines the ratio of  $\beta_{\text{sed,ref}}$  to  $\beta_{\text{TP,ref}}$  one finds that sedimentation would ultimately dominate the

long-time coagulation behavior. However, one can show that, as long as the population SMD is less than about :

$$\text{SMD}_{\text{crit}} = \nu_g \left( \|\nabla \ln T\| \frac{\rho_g/\rho_p}{g_{\text{eff}}} \right)^{1/2} \quad (23)$$

then the differential sedimentation mechanism can be neglected. Of course, this condition is readily met when the effective “ $g_{\text{eff}}$ ” is small.

#### D. Non-Continuum Effects

When the Knudsen numbers  $\text{Kn}_1$  and  $\text{Kn}_2$  are not small then the Brownian- and thermophoretic coagulation rate constants are both affected, but in opposite directions.

The Brownian coefficient is increased because the relative Brownian diffusivity  $D_1 + D_2$  is increased by the relevant Cunningham-Millikan- Stokes drag (“slip”) correction factors.

However,  $\beta_{\text{TP}}$  is reduced because of the reduced sensitivity of the dimensionless thermophoretic diffusivity  $\tilde{\alpha}$  to size as one approaches the “free-molecule” limit ( $\text{Kn} \rightarrow \infty$ ). These “rarefaction” effects would be straightforward to include in an extended theory, at the expense of introducing the gas mean-free-path :SMD ratio as an additional parameter. Indeed, for the high  $\|\nabla T\|$ , atmospheric pressure Fe(L)/He “mist” examples cited in Rosner and Arias-Zugasti (2011) [4]  $\text{Kn}$ -values were not small enough to maximize the coagulation consequences of particle thermophoresis. Nevertheless, we estimated that this mechanism probably dominated the encounter rate between particles straddling the nominal diameter of 1 micrometer.

#### E. Dense Vapor Effects

Particle thermophoretic drift velocities outside of the domain of ideal gas kinetic theory remain an open question (see, e.g., Rosner (2011) [1]). For small departures from ideality, as relevant to high pressure laminar diffusion flames, the approach of Rosner and Arias-Zugasti (2007) [25] (based on the virial EOS together with the Thermodynamics of Irreversible Processes) appears to be promising, but remains to be developed. However, extensions to higher carrier vapor molecular volume fractions ( $> O(10^{-1})$ ) will be needed to properly deal with supercritical fluid particle processing applications (Rosner and Arias-Zugasti (2011) [7])—especially in the presence of simultaneous temperature gradients.

### VII. IMPLICATIONS, CONCLUSIONS, GENERALIZATIONS, FUTURE WORK

The nucleation of condensable vapors often occurs due to supersaturations achieved in the presence of strong temperature gradients (see, e.g., Turkdogan and Mills (1964) [2], and Katz (1967) [26]). Yet, such data have previously been analyzed on the basis of homogeneous nucleation theory and coagulation rate theory based on locally uniform temperatures. This observation has motivated our present theoretical study of the coagulation-rate consequences of spatially non-uniform temperature.

Here we consider for the first time the simultaneous role of size-dependent thermophoresis and continuum regime Brownian diffusion in shaping “coagulation-aged” (asymptotic-) aerosol particle size distributions. In contrast to the extreme case of initial thermophoretic “domination” (Rosner and Arias-Zugasti (2011) [4]), our present methods and results apply to more general situations often encountered for smaller temperature gradients ( $< 10^5$  K/m), where size-dependent thermophoretic drift modifies but does not initially dominate the coagulation frequency. As described in Section III, we have avoided using an “additive kernel” approximation by basing our combined kernel on the solution of a test particle convective-diffusion equation which accounts for both ordinary Brownian diffusion and (thermophoretic) drift. This kernel is then introduced into a Smoluchowski-type population-balance integro-PDE, so that we can track the evolution of initially log-normal distributions in a locally non-isothermal gas environment. As expected, when a reference Peclet number of the form :  $\beta_{\text{TP,ref}}/\beta_{\text{B,ref}}$  is much smaller than, say 0.1, we recover the previously well-studied/characterized Brownian self-preserving populations, with a diameter-based geometric standard deviation near 2.4. However, for intermediate Peclet-values characteristic distortions set in, corresponding to increased spread and skewness, and slightly smaller departures from log-normality. Ultimately (for Peclet-values larger than about 10) our quasi-self-preserving DSDs become indistinguishable from our previously reported thermophoretically-dominated results (Rosner and Arias-Zugasti (2011) [4]).

Remarkably, it has been observed that, for  $k_p/k_g > 10$ , the dependence on the particle/gas Fourier thermal conductivity ratio reduces to a slight modification of the characteristic time and size scales, and hence the results for the self-similar normalized distribution function reached in the long-time limit are almost independent of the particle/gas Fourier thermal conductivity ratio in the whole range of values of the Peclet number.

In view of the idealizations we have chosen to introduce, in Section VI we provide quantitative validity criteria and indicate promising routes to further generalizations. These extensions are expected to be essential to make particle processing predictions in yet-more demanding environments (e.g., high-pressure flames and supercritical fluids—which are the focus of our current attention).

## ACKNOWLEDGMENTS

This study was supported by NSF under Grant : CBET-1037733 to Yale University. MAZ also gratefully acknowledges grants by Ministerio de Ciencia e Innovación (#ENE2008-06515-C04-03) and Comunidad de Madrid (#S2009/ENE-1597) at UNED.

- 
- [1] D. E. Rosner, *Progress in Energy and Combustion Science*, Submitted (2011).
  - [2] E. T. Turkdogan and K. C. Mills, *Transactions of the Metallurgical Society of AIME* **230**, 750 (1964).
  - [3] T. Kumada, R. Ishiguro, and F. Kasahara, *Journal of Nuclear Science and Technology* **15**, 912 (1978).
  - [4] D. E. Rosner and M. Arias-Zugasti, *Physical Review Letters* **106**, 015502 (2011).
  - [5] S. Simons, M. M. R. Williams, and J. S. Cassell, *Journal of Aerosol Science* **17**, 789 (1986).
  - [6] S. K. Friedlander, *Smoke, Dust and Haze—Fundamentals of Aerosol Dynamics* (Oxford University Press, Oxford UK, 2000).
  - [7] D. E. Rosner and M. Arias-Zugasti, *AIChE J* **57**, 307 (2011).
  - [8] R. McGraw, *Aerosol Science and Technology* **27**, 255 (1997).
  - [9] M. Arias-Zugasti, *Journal of Aerosol Science* **37**, 1356 (2006).
  - [10] M. Arias-Zugasti, *Journal of Aerosol Science* (2011), in prep.
  - [11] D. E. Rosner, *Transport Processes in Chemically Reacting Flow Systems* (DOVER, Mineola NY, 2000).
  - [12] D. E. Rosner and M. Arias-Zugasti, *Industrial & Engineering Chemistry Research* (2011), invited Paper for Churchill 90 issue. In press.
  - [13] L. Talbot, R. K. Cheng, R. W. Schefer, and D. R. Willis, *Journal of Fluid Mechanics* **101**, 737 (1980).
  - [14] E. Sajo, *Aerosol Science and Technology* **42**, 134 (2008).
  - [15] E. Sajo, *Aerosol Science and Technology* **44**, 916 (2010).
  - [16] J. P. Boyd, *Chebyshev and Fourier Spectral Methods*, 2nd ed. (DOVER, Mineola NY, 2000).
  - [17] J. C. Barrett and N. A. Webb, *Journal of Aerosol Science* **29**, 31 (1998).
  - [18] Ramkrishna, *Population Balances: Theory and Applications to Particulate Systems in Engineering* (Academic Press, New York, 2000).
  - [19] S. Vemury and S. E. Pratsinis, *Journal of Aerosol Science* **26**, 175 (1995).
  - [20] P. N. Singh and D. Ramkrishna, *Journal of Colloid and Interface Science* **53**, 214 (1975).
  - [21] K. J. Sampson and D. Ramkrishna, *Journal of Colloid and Interface Science* **103**, 245 (1985).
  - [22] M. Strumendo and H. Arastoopour, *Chemical Engineering Science* **63**, 2624 (2008).
  - [23] M. Strumendo and H. Arastoopour, *Industrial & Engineering Chemistry Research* **48**, 262 (2009).
  - [24] A. V. Filippov, M. Zurita, and D. E. Rosner, *Journal of Colloid and Interface Science* **229**, 261 (2000).
  - [25] D. E. Rosner and M. Arias-Zugasti, *AIChE J* **53**, 1879 (2007).
  - [26] J. L. Katz and B. J. Ostermier, *Journal of Chemical Physics* **47**, 478 (1967).